Underlying role of mechanical rigidity and topological constraints in physical sputtering and reactive ion etching of amorphous materials

Gyanendra Bhattarai, Shailesh Dhungana, Bradley J. Nordell, Anthony N. Caruso, Michelle M. Paquette, William A. Lanford, and Sean W. King

Phys. Rev. Materials **2**, 055602 — Published 10 May 2018

DOI: 10.1103/PhysRevMaterials.2.055602

The Underlying Role of Mechanical Rigidity and Topological Constraints in Physical Sputtering and Reactive Ion Etching of Amorphous Materials

Revised 4/23/2018 13:00:00

Gyanendra Bhattarai,[1] Shailesh Dhungana,[1] Bradley J. Nordell,[1] Anthony N. Caruso,[1] Michelle M. Paquette,[1] William A. Lanford,[2] Sean W. King[3]

[1]*Department of Physics and Astronomy, University of Missouri-Kansas City, Kansas City, MO 64110, USA*
[2]*Department of Physics, University at Albany, Albany, NY 1222, USA*
[3]*Logic Technology Development, Intel Corporation, Hillsboro, OR 97124, USA*

Analytical expressions describing ion-induced sputter or etch processes generally relate the yield to the surface atomic binding energy (U_{sb}) for the target material. While easy to measure for the elements, U_{sb} is more complicated to establish for amorphous and multi-element materials due to composition-driven variations and incongruent sublimation. In this regard, we show that for amorphous multi-element materials, the ion-driven yield can instead be better understood via consideration of mechanical rigidity and network topology. We first demonstrate a direct relationship between U_{sb}, bulk modulus, and ion sputter yield for the elements, and then subsequently prove our hypothesis for amorphous multi-element compounds by demonstrating that the same relationships exist between the reactive ion etch (RIE) rate and nanoindentation Young's modulus for a series of a-SiN_x:H and a-SiO_xC_y:H thin films. The impact of network topology is further revealed via application of the Phillips–Thorpe theory of topological constraints, which directly relates Young's modulus to the mean atomic coordination ($\langle r \rangle$) for an amorphous solid. The combined analysis allows the trends and plateaus in the RIE rate to be ultimately reinterpreted in terms of the atomic structure of the target material through consideration of $\langle r \rangle$. These findings establish the important underlying role of mechanical rigidity and network topology in ion–solid interactions and provide a new consideration for the design and optimization of radiation-hard materials in nuclear and outer space environments.

Keywords: sputter, etch, amorphous, topological constraint, modulus, rigidity
PACS: 95.55.Sh, 93.90.+y, 13.15.+g

I. INTRODUCTION

Understanding the physical mechanisms involved in the interaction between energetic ions and solid materials is crucial for predicting the behavior of a variety of important technological processes and applications, ranging from microelectronic device fabrication and reliability [1], to nuclear fusion and fission [2,3], to low earth orbit and interstellar travel [4]. However, a fundamental understanding of these processes at a level sufficient to predict their behavior is still lacking in many cases. As one example, the ion-induced sputtering and etching of materials are two techniques widely utilized for precision deposition and patterning of thin-film materials in microelectronic device fabrication [5,6]. However, the influence of target material propertes on ion–solid interactions is still not well understood: it is accounted for theoretically only through a macroscopic surface atomic binding energy (U_{sb}) term. While U_{sb} is a well-documented property for most elemental materials, it is more difficult to define and experimentally quantify for multi-element and compound materials due to composition-driven variations in U_{sb} [7], incongruent sublimation [7], and preferential sputtering [8,9]. It is particularly challenging to define for amorphous and/or hydrogenated materials where significant bond rearrangement and/or hydrogen loss may occur before other constituents exhibit any volatility [10].

In this regard, we postulate that U_{sb} can be directly related to the mechanical rigidity of a material, and ultimately its atomic structure, through established relations between cohesive energy (*CE*), bulk modulus (*BM*), Young's modulus (*YM*), and mean atomic coordination ($\langle r \rangle$) [11]. The latter are more experimentally quantifiable properties for multi-component and amorphous materials, and should allow the extension and application of various sputter/etch theories to these. To validate our hypotheses, we first analytically illustrate the direct relationship that exists between U_{sb}, *CE*, *BM*, and *YM* for materials with pure ionic bonding. Using published values, we demonstrate that the derived relationships hold experimentally for both pure ionic and covalent materials. We then use standard sputtering theories and established sputtering yield values for the covalent elements to demonstrate the expected connection between sputter yield (*Y*), *BM*, and *YM*.

To further establish the underlying influence of atomic structure on ion-driven sputter/etch rates, we additionally

employ the Phillips–Thorpe theory of topological constraints to illustrate the direct connection that exists between $\langle r \rangle$, *YM* and—by extension—U_{sb} [12,13]. To experimentally demonstrate these relationships and support our hypotheses for multi-element amorphous hydrogenated systems, we have experimentally examined the relationship between the reactive ion etch (RIE) rates for a series of a-SiN_x:H and a-SiO_xC_y:H thin films and their *YM* (as determined by nanoindentation) and $\langle r \rangle$ (derived from elemental composition determined through combined Rutherford backscattering spectroscopy (RBS) and nuclear reaction analysis (NRA) measurements). For the specific SiN_x:H and SiO_xC_y:H thin films investigated, the selected RIE chemistry exhibits a strong physical (i.e., sputtering) component [14], thus allowing extension of standard sputtering theories and the demonstration of a direct connection between etch rate, *YM*, and $\langle r \rangle$. We conclude by discussing how the observed trends could have an impact on the design and optimization of new radiation-hard materials for microelectronic, nuclear detection/fission, and outer space cladding material applications.

II. SURFACE BINDING ENERGY (U_{SB}) & BULK MODULUS (*BM*) THEORY

To establish a direct connection between U_{sb} and *CE*, we first note that U_{sb} is typically equated to the heat/enthalpy of sublimation (H_{sub}) for the target material divided by Avogadro's number [15]. We further note that H_{sub} and *CE* are essentially identical properties where H_{sub} is defined as the energy needed to convert a certain amount of material from a solid directly into a vapor, and *CE* is instead defined as the energy needed to break all bonds and completely separate the atoms in the material (i.e., vaporize the entire material) [11]. To establish the connection between *CE* and *BM*, we note that for ionic materials the bonding can be accurately described by considering only point charge Coulombic attractive forces and repulsive electron cloud forces, leading to the following analytical expressions for *CE* and *BM*:

$$CE = \frac{\beta e^2}{x_0}\frac{m-1}{m}; \qquad \beta = \frac{\alpha}{4\pi\epsilon_0} \#(1)$$

$$BM = \frac{\beta e^2}{18 x_0^4}(m-1) \#(2)$$

where α = the Madelung constant, x_0 = the equilibrium separation between the cation and anion, and *m* = an exponent describing the electron cloud repulsive forces (typically ranging between 6 and 12) [11]. As the influence of *m* on *CE* is relatively small, *m* can be treated as a constant to allow the combination of (1) and (2) through x_0, leading to the following general relation:

$$BM \propto CE^4 \propto H_{sub}^4 \#(3)$$

Using literature values for H_{sub} and *BM* [16,17], we show in Figure 1 that relationship (3) holds for both classic ionically bonded alkali halide materials (coefficient of determination, R^2 = 0.93, Fig. 1a) as well as for the column IV elements that exhibit pure covalent bonding (R^2 = 0.95, Fig. 1b) [18-20]. For the latter, we note that a simple analytical expression describing *CE* and *BM* for pure covalent materials does not exist and more complicated methods are needed to provide estimates for both [21]. However, Fig. 1b clearly demonstrates the analytical relationship between H_{sub} and *BM* derived for ionic materials still empirically holds for covalent materials.

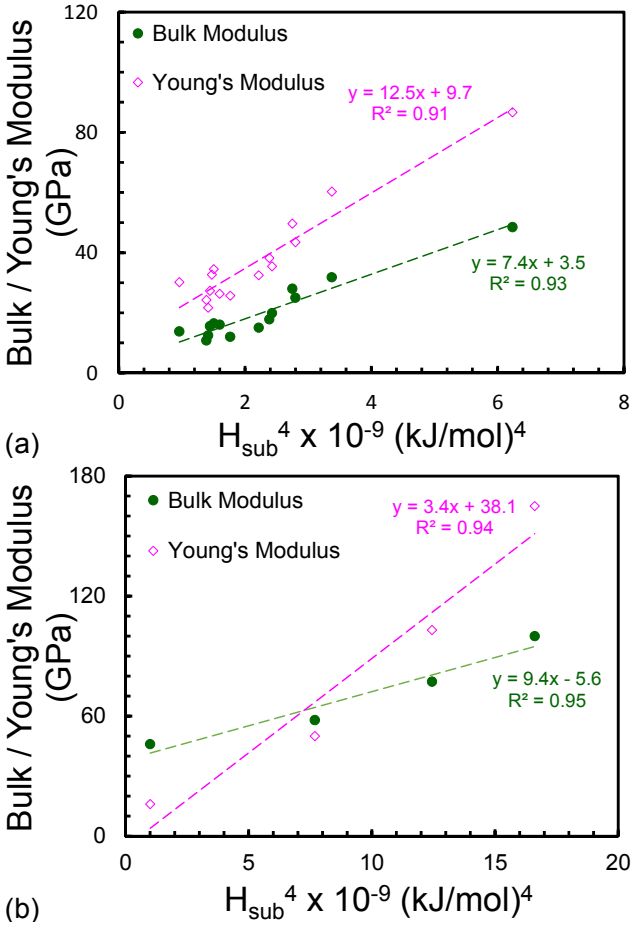

FIG. 1. (Color online) Bulk or Young's modulus (GPa) vs. enthalpy of sublimation (H_{sub}) in kJ/mol for (a) alkali halides and (b) group IV elements. Note: carbon excluded from Fig. 1b due to the 2D structure exhibited by graphite and a lack of published H_{sub} data for carbon in the 3D diamond structure exhibited by Si, Ge, and Sn.

As Young's modulus is directly related to *BM* through Poisson's ratio (ν), that is *YM* = 3*BM*(1–2ν) [11], one can

similarly show that YM should also be proportional to H_{sub}^4. This is clearly shown in Fig. 1 for both the alkali halides and the column IV elements. For the a-SiN_x:H and a-SiO_xC_y:H materials to be investigated later, the atomic bonding is of mixed ionic–covalent character [22]. Based on the relationships observed in Fig. 1, we therefore conclude that a similar relationship between U_{sb}/H_{sub} and BM/YM should be expected.

III. SPUTTER YIELD (Y) THEORY

Most theories describing the relationship between ion energy, material properties, and sputter yield lead to analytical expressions of similar form to that originally derived in Sigmund's collisional cascade theory [23,24], which relates sputter yield (Y) to the projectile ion energy (E) and the surface atomic binding energy (U_{sb}) of the target material. For ion energies less than 1 keV, Sigmund's yield expression specifically takes the form [15]:

$$Y = \frac{3}{4\pi^2}\sigma\gamma\frac{E}{U_{sb}} \#(4)$$

where σ is a dimensionless correction factor that depends on the ratio of the target atom mass (m_2) to the mass of the projectile ion (m_1) and γ is the energy transfer factor between the projectile ion and target atom, taken as $4m_1m_2/(m_1+m_2)^2$. Other sputtering theories such as the simplified collisional model of Mahan [25] and the molecule/cluster models of Urbassek [26] and Belyk [27] maintain the same general form as the Sigmund yield expression, but predict slightly different exponents for U_{sb} of –0.5 and –1.5, respectively.

To establish a direct connection between bulk modulus and ion-induced sputter yield, one can combine (1) and (4) through U_{sb} where the U_{sb}^{-1} dependence leads to:

$$\frac{Y}{\gamma\sigma E} \propto BM^{-\frac{1}{4}} \#(5)$$

However, as mentioned previously, other theories have predicted sputter yield to exhibit different dependencies on U_{sb}. Specifically, the simplified collision model of Mahan predicts a $U_{sb}^{-0.5}$ dependence while the molecule/cluster sputtering models of Urbassek [26] and Belyk [27] predict a $U_{sb}^{-1.5}$ dependence. These would instead lead to $Y \propto BM^{-1/8}$ and $BM^{-3/8}$, respectively.

Empirically, Mahan [15] has shown using the 1 keV Ar^+ sputter yield data of Matsunami [28] that Y is $\propto U_{sb}^{-1.3}$, which is in reasonable agreement with the exponent predicted by the molecule/cluster sputter models of Urbassek [11] and Belyk [12]. In this regard, we do note that atomic clusters are a commonly observed, but minor component of the yield from sputter processes [29,30]. As noted by Mahan, the empirically observed higher exponent may stem from the Matsunami data being collected in the nonlinear cascade regime, whereas the simplified collisional and other models are valid only in the linear cascade regime where the ejection of just a single atom is considered [25]. In either case, $Y \propto BM^{-1/3}$ would be predicted based on this empirical relationship.

However, Mahan's empirical Y vs. U_{sb} analysis was heavily weighted by metallic materials, which have a different functional dependence between BM and CE/U_{sb} [31,32]. Therefore, we present in Figure 2a a similar plot of the Matsunami data considering only the column IV elements sputtered by 1 keV Ar^+ ions. As can be seen, a slightly higher exponent of –1.5 with $R^2 = 0.8$ was found. This exponent is again in excellent agreement with that predicted by Urbassek and Belyk [11,12] and likely a result of the column IV sputter yield data also being collected outside of the linear cascade regime (i.e., non-linear cascade or projectile penetration regimes) [15]. As for the Urbassek-Belyk theory, one would then empirically predict the sputter yield to also vary with BM/YM raised to the ~ –0.375 power based on our model.

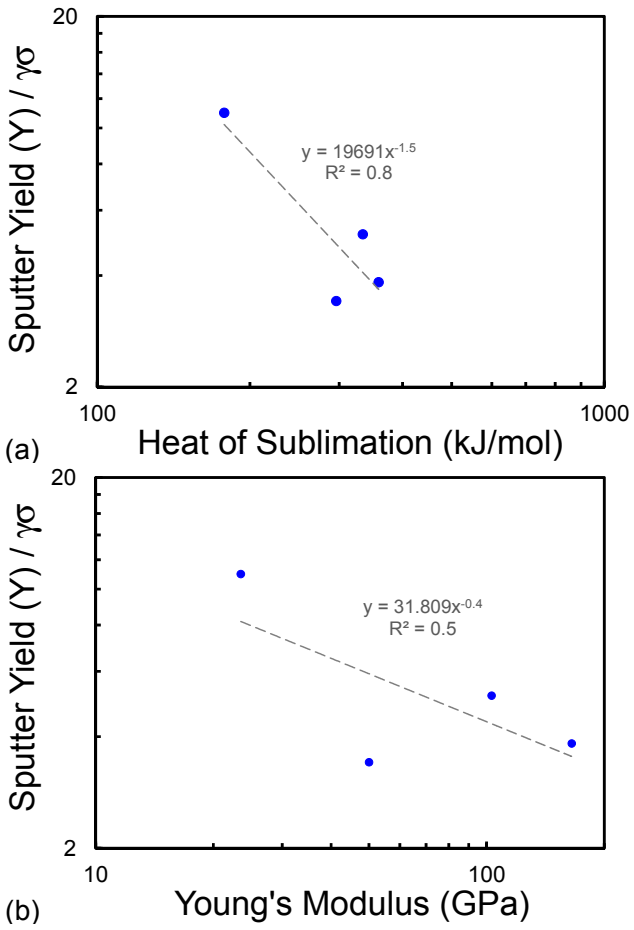

FIG. 2. (Color online) 1 keV Ar^+ sputter yield values for column IV elements (excluding carbon) [7] versus (a) heat of sublimation and (b) Young's modulus.

As shown in Fig. 2b, the expected exponential dependence of Y on YM does exist. Power law fitting of the same column IV Ar^+ sputter yield data plotted now versus Young's modulus indicates an exponent of –0.4 in strong agreement with the predicted value of –0.375 but with a reduced R^2 of 0.5, indicating that only 50% of the variability in Fig. 2b was accounted for. The reduced R^2 may be due to the low sample size created by considering only the group IV covalent elements, or could be due to the above analysis for pure ionic materials not accurately extending to pure covalent materials. For the latter case, we do note that we were not able to perform a similar analysis to Fig. 2 for pure ionic materials due to an inability to identify a reasonably sufficient sputter yield data set in the literature. However, we do note that in the field of sputtering, "good" agreement is typically considered to be within a factor of 2 [15]. Fig. 2b therefore motivates extension of the previously developed theory to other processes and material systems where ion–surface interactions are involved and stronger correlations may be observed.

Having supported our initial hypothesis that sputter yields can be related to the target materials' mechanical rigidity using established sputter yield data, we next seek to further support our hypothesis for multi-element materials by examining the reactive ion etch (RIE) rates and YM of a-SiN_x:H and a-SiO_xC_y:H thin film materials. We further seek to establish and demonstrate a direct connection between RIE rates and atomic structure via analytically and experimentally examining the dependence between mean atomic coordination ($\langle r \rangle$) and YM for these materials.

IV. EXPERIMENTAL

The growth, characterization, and reactive ion etch rate measurements for the a-SiN_x:H and a-SiO_xC_y:H thin films investigated in this study have been previously described in detail [14]. Briefly, all films were deposited on 300 mm diameter Si (001) substrates via plasma-enhanced chemical vapor deposition (PECVD) using various combinations of silanes, organosilanes, ammonia, nitrogen, hydrogen, and gaseous oxidizers [33]. To remove additional complexities related to the possible presence of interconnected nano-porosity, as discussed in a preceeding publication [14] and other investigations [34,35], the a-SiN_x:H and a-SiO_xC_y:H films selected for this study exhibited zero interconnected porosity as determined by ellipsometric porosimetry methods [36].

The mechanical properties (YM and hardness (H)) for the various thin films in this study were determined by previously described nanoindentation measurements [37]. The full elemental composition for the films was determined by combined nuclear reaction analysis (NRA) and Rutherford backscattering spectroscopy (RBS) measurements [38]. The mean atomic coordination ($\langle r \rangle$) for each film was calculated directly from the elemental compositions determined by NRA-RBS assuming atomic coordinations of 4, 4, 3, 2, and 1 for Si, C, N, O, and H, respectively [39].

The RIE rate measurements were performed by exposing the samples to a plasma-activated CHF_3 chemistry and measuring differences in the step heights created between masked and unmasked portions of the films [14]. The etch times were targeted such that steady state etching conditions were achieved. We note that while there is a chemical component to the CHF_3 RIE associated with reactive fluorine and other neutral radicals created in the RF plasma [14,40], the process is primarily driven by physical sputtering and surface intermixing resulting from interactions with the various energetic ion species also present [41,42]. More specifically, the CHF_3 plasma leads to the formation of an adsorbed/co-deposited CF_x surface layer on the target film. Etching (or reactive sputtering) is believed to occur via ion-assisted surface bombardment which drives chemical intermixing between the fluorinated layer and the underlying film and also helps to liberate surface fluorine species and other etch products [41,42]. More detailed descriptions and simulations of the neutral and ion-surface mechanisms involved in fluorine based RIE processes are provided in [43-49].

The presence of a complex fluorinated surface layer during RIE may cause one to question the validity of applying the preceding analysis to correlate RIE rates to a "bulk" material property such as Young's modulus. However, a related amorphous surface layer is also well known to form during sputtering of crystalline materials [25]. Based on the preceding analysis presented in Fig. 2, we therefore posit that the mechanical properties of any surface layers formed during sputtering or plasma etching are directly proportional to those of the underlying film or substrate. This is supported by prior correlations relating the sputter yields of the elements to surface binding energies (U_{sb}) computed from "bulk" sublimation energies [25]. Further, the influence of other bulk properties on dry etch rates such as interconnected nano-porosity have been previously discussed [34,35]. Lastly, it is well known in thin film nano-indentation measurements that the underlying substrate can heavily influence the measured indentation response which is a complex function of the mechanical properties for both the film and substrate [50]. More specifically, the apparent mechanical properties extracted from an indentation measurement can approach those of the substrate as the film thickness decreases / indentation depth increases [50]. By analogy, one can then anticipate that in ion-surface collisions involving a few atomic layer thick fluorinated or amorphous surface layer that the mechanical stiffness an ion experiences on collision will be largely those of the film/substrate.

V. RIE RATE AND YOUNG'S MODULUS (*YM*) CORRELATION

Figure 3 presents the measured CHF_3 RIE rates for (a) a-SiN_x:H and (b) a-SiO_xC_y:H as a function of nanoindentation *YM*. For both materials, the CHF_3 RIE rates are observed to increase with decreasing *YM*. Previously [14], we have shown a qualitative correlation between the CHF_3 RIE rate and the hydrogen content and mass density for a-SiN_x:H and a-SiO_xC_y:H (see Supplemental Material [51]). Due to the well known dependence of *YM* on hydrogen content and mass density [52-54], one could qualitatively predict the trends observed in Fig. 3 based on these prior observations. However, we demonstrate here a quantitative relationship between etch rate and *YM* as predicted by the preceeding analysis leading to relation (5). Specifically, a power law fit to the experimental data in Fig. 3 indicates an exponent of –0.6 and –0.4 for a-SiN_x:H and a-SiO_xC_y:H, respectively, with persuasive R^2 values of 0.7. These exponent values are in good agreement with those empirically observed previously for 1 keV Ar^+ sputtering of the column IV elements.

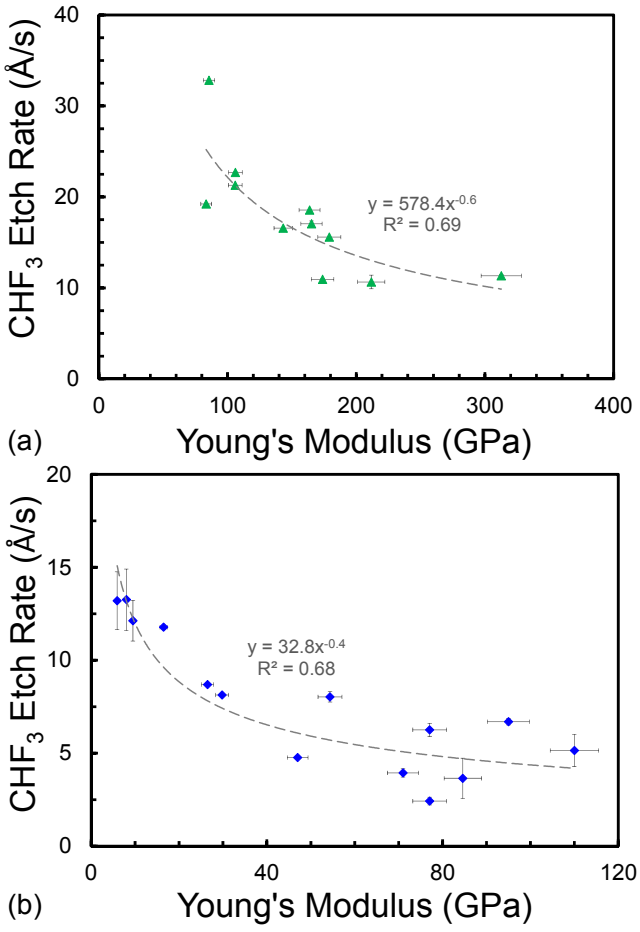

FIG. 3. (Color online) CHF_3 RIE rate vs. Young's Modulus (*YM*) for (a) a-SiN_x:H and (b) a-SiO_xC_y:H. Note: the CHF_3 etch rate error bars represent a one-sigma standard deviation for measurements performed on 2–5 identical samples exposed to the same CHF_3 chemistry. A lack of error bars indicates either that only a single data point was used or that the standard deviation was smaller than the data point marker. The *YM* error bars represent a one-sigma standard deviation calculated from 10 indentations performed on one sample.

The fitted exponents in Fig. 3 are also in good agreement with the exponent of –3/8 theoretically predicted for sputtering of molecule/cluster species [31,32]. In this regard, we do acknowledge that while atomic clusters are typically observed to be a minor component of the yield from sputtering processes [55], for plasma etching processes the yield/etch products are primarily molecular [56]. Thus, the agreement between the U_{sb} exponents observed in Fig. 3 and those predicted by the molecule/cluster sputtering theories corroborates the plasma etch products being molecular species as opposed to atomic species. Although not shown, we do note that virtually identical trends between RIE rates and nanoindentation hardness were also observed.

VI. *YM, RIE RATE* AND MEAN COORDINATION ($\langle r \rangle$)

Having established in the preceding sections a direct relation between ion-driven removal rates and mechanical rigidity, we next seek to establish a direct connection between etch rate and atomic structure via consideration of the Phillips–Thorpe topological constraint theory (TCT) for amorphous materials. TCT views amorphous materials as a Maxwellian system of trusses where each chemical bond represents a strut or physical constraint [57,58]. The resistance to mechanical deformation for an amorphous material can then be evaluated based on Maxwell's stability criterion where the number of constraints per atom (n_c) is weighed against the degrees of freedom per atom (n_f). TCT thus predicts that for $n_c < n_f$, the system is underconstrained and mechanically unstable/flexible, while for $n_c > n_f$ the system is mechanically stable but overconstrained and stressed/rigid [58]. At $n_c = n_f$, amorphous materials are considered to be isostatic and optimally constrained with unique "intermediate phase" properties [59].

For a three dimensionally networked system, $n_f = 3$ and the constraints arise from the two- and three-body interactions necessary to maintain the bond lengths and bond angles at their mean values. The number of bond stretching (δ) and bond bending (θ) constraints for each atom can be directly calculated based on its coordination number, r. For $r \geq 2$, it can be specifically shown that $\delta = r/2$ and $\theta = 2r - 3$ [13]. In turn, it can also be shown that n_c is a direct function of the mean atomic coordination ($\langle r \rangle$) for the system and that the isostatic point corresponds to a critical mean atomic coordination ($\langle r \rangle_c$) [58].

For tetrahedrally networked systems, $\langle r\rangle_c$ has been shown to be 2.4 [58,60]. It has been additionally shown that for underconstrained systems, mechanical rigidity should be invariant with $\langle r\rangle < \langle r\rangle_c$. However for overconstrained systems, rigidity should percolate through the system with increasing $\langle r\rangle$ above $\langle r\rangle_c$ to the 3/2 power [61,62]. That is, for mechanical properties such as indentation Young's modulus (*YM*) and hardness (*H*), one would expect *YM* or *H* to be $\propto (\langle r\rangle - \langle r\rangle_c)^{3/2}$. In prior publications [39,63], we have experimentally demonstrated for a-SiC:H materials the existence of both the predicted critical point at $\langle r\rangle_c = 2.4$ and the 3/2 scaling for $\langle r\rangle > 2.4$. In Figure 4, we demonstrate the same for both the a-SiN_x:H and a-SiO_xC_y:H materials investigated in this study. The dash-dot line in Fig. 4 represents a fit to the experimental *YM* vs. $\langle r\rangle$ plot based on linear regression analysis of $YM^{2/3}$ vs. $(\langle r\rangle - \langle r\rangle_c)$. The dashed vertical line signifies the isostatic point where $\langle r\rangle = \langle r\rangle_c = 2.4$. Also included in Fig. 4 are the literature reported values for the *YM* of single crystalline Si_3N_4 and SiO_2 (quartz) [64,65].

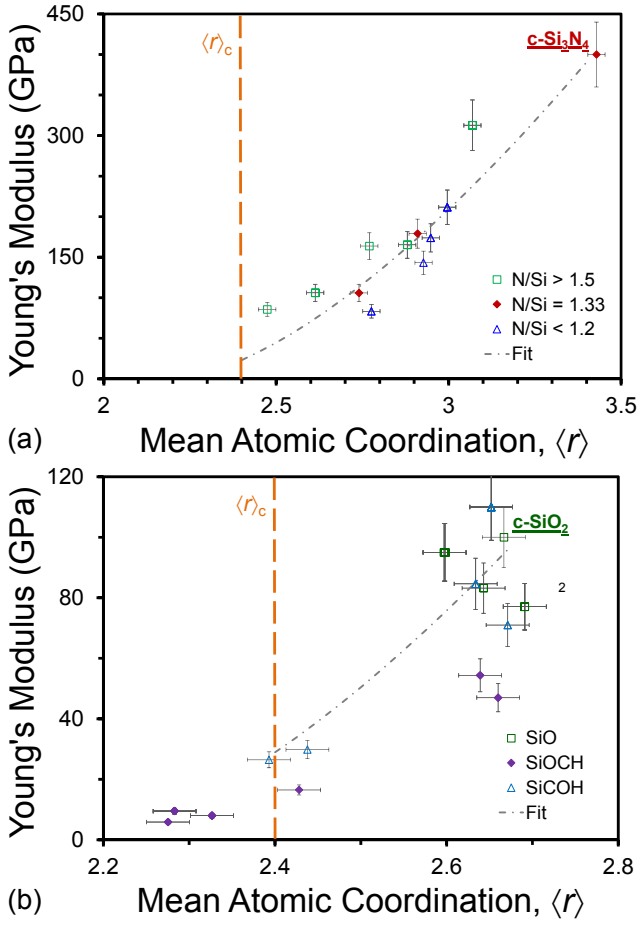

FIG. 4. (Color online) Nanoindentation Young's modulus versus mean atomic coordination ($\langle r\rangle$) for (a) a-SiN_x:H, and (a) a-SiO_xC_y:H.

Examining Fig. 4a closely, one can see that there is some scatter in the data that correlates with the N/Si stoichiometry in the films. Specifically, the experimental data points for the a-SiN_x:H films where the N/Si ratio was significantly greater than the stoichiometric value of 1.33 lie on the high side of the fit whereas those for films where N/Si is < 1.2 lie below the fit. This can be understood as both rigidity percolation due to changes in mean atomic coordination and percolation of Si–Si vs. Si–N network bonding through the material. For a-SiN_x:H films with N/Si < 1.2, Si–Si and Si–N network bonding both percolate through the system and *YM* falls below the fit in Fig. 4a due to the reduced stiffness of Si–Si bonds relative to Si–N bonds [64,66]. For N/Si ≥ 1.33, Si–N network bonding exclusively percolates throughout the system and hence the *YM* values are slightly higher. In either scenario, *YM* does decrease with decreasing $\langle r\rangle$ as predicted by the Phillips–Thorpe TCT. However, the predicted inflection point in *YM* at $\langle r\rangle = \langle r\rangle_c$. cannot be observed in Fig. 4a due to a lack of a-SiN_x:H films with $\langle r\rangle < 2.4$ available for this study.

For a-SiO_xC_y:H, thin films with $\langle r\rangle < \langle r\rangle_c$ were obtained, and as can be seen in Fig. 4b, a low variance in *YM* for $\langle r\rangle < 2.4$ is also observed. Unfortunately, a less satisfying correlation between *YM* and $\langle r\rangle$ for $\langle r\rangle > \langle r\rangle_c$ is observed compared to that shown in Fig. 4a. However, this can be similarly attributed to differences in the stoichiometries of the various a-SiO_xC_y:H thin films investigated, the significant differences in stiffness for SiO_2 vs. SiC, and the presence of some nitrogen impurities in the PECVD SiO_2 films. For the former, we have denoted in Fig. 4b those films for which Si–O–Si bonding dominates as SiOCH and those for which both significant Si–O–Si and Si–C–Si bonding exists as SiCOH based on previously described FTIR measurements [14]. Due to the higher stiffness of SiC relative to SiO_2, the SiCOH films have higher *YM* relative to the SiO_2 and SiOCH films in Fig. 4a [39,65]. Similarly, the presence of ~4% nitrogen impurities in some of the PECVD SiO_2 films (from the N_2O oxidizer [67]) contributes to their *YM* exceeding that of single crystal SiO_2 (quartz) due to the higher stiffness of Si–N bonding [64].

Having established theoretically and experimentally the connection between atomic structure and mechanical properties, we next examine the influence of atomic structure (i.e., $\langle r\rangle$) on the previously presented CHF_3 RIE rates. Based on the molecule/cluster sputter model where a $YM^{-3/8}$ dependence was predicted [26,27] and the $YM \propto (\langle r\rangle - \langle r\rangle_c)^{3/2}$ prediction from Phillips–Thorpe TCT [12,13], one would in turn expect the sputter/etch rate to exhibit a $(\langle r\rangle - \langle r\rangle_c)^{9/16}$ dependence. To illustrate such a dependence, we have replotted in Figure 5 the measured CHF_3 RIE rates as a function of $\langle r\rangle$ for both the a-SiN_x:H and a-SiO_xC_y:H thin films. For a-SiN_x:H, we observe a clear increase in RIE rate as $\langle r\rangle$ decreases as anticipated, and power law fitting of the data plotted versus $\langle r\rangle - \langle r\rangle_c$ yields an exponent of –0.5 with a convincing R^2 of 0.8. The former is in excellent

agreement with the –9/16 value predicted by the combined molecule/cluster sputter and Phillips–Thorpe TCT theories. The latter represents an improvement over the R^2 of 0.7 observed for the a-SiN_x:H RIE rate vs. Young's modulus correlation in Fig. 3a.

For the a-SiO_xC_y:H CHF_3 RIE data, power law fitting yielded a much lower R^2 value of 0.4, indicating that only 40% of the variability was captured by the model. This is likely due to the $\langle r\rangle > \langle r\rangle_c$ data being effectively clustered into two separate distributions with significant scatter. Additional RIE rate data in the range of $\langle r\rangle$ = 2.4 – 2.6 would be needed to convincingly assess the strength of correlation. Nevertheless, the fitted exponent of –0.4 is still in reasonable agreement with the predicted value of –9/16 and does not contradict the developed theory.

Perhaps more noteworthy though is the apparent leveling off in CHF_3 RIE rates for a-SiO_xC_y:H at $\langle r\rangle < 2.4$ which is the $\langle r\rangle_c$ predicted by Phillips–Thorpe TCT for a tetrahedral coordinated system [12]. The observed possible plateau in CHF_3 RIE rate is consistent with the predictions of the Phillips–Thorpe TCT that mechanical properties should be invariant with $\langle r\rangle$ for $\langle r\rangle < \langle r\rangle_c$. This supports the connection between plasma etching and atomic structure, and further underscores both the underlying role of mechanical rigidity and atomic structure in ion-driven sputtering and etch processes.

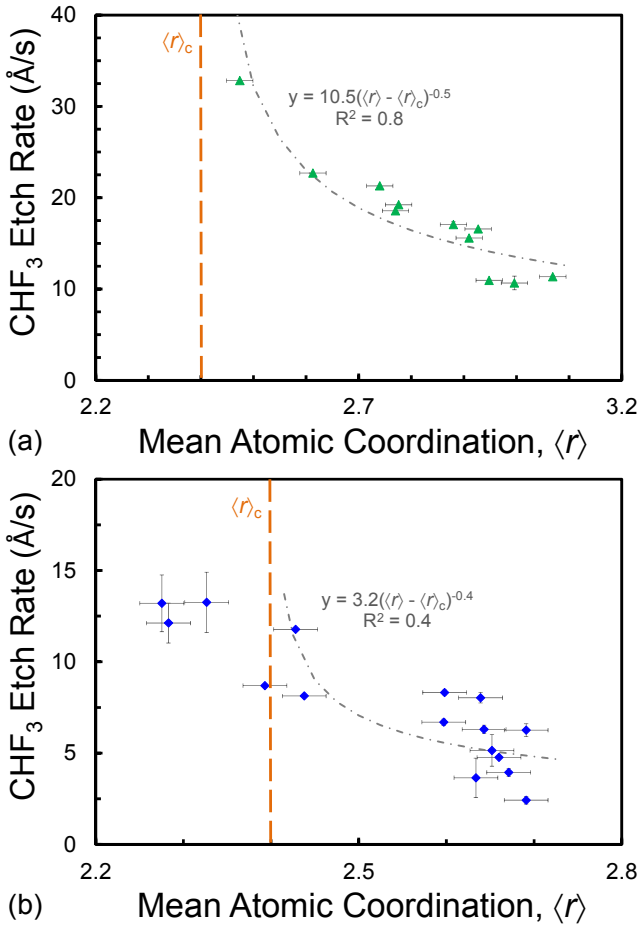

FIG. 5. (Color online) CHF_3 RIE rates versus mean network coordination ($\langle r\rangle$) for (a) a-SiN_x:H, and (b) a-SiO_xC_y:H.

VII. DISCUSSION

We acknowledge that experimental verification of the presented scaling theory in some cases is limited by a narrow data set and correlation coefficients that capture only 50% of the observed variability. However, the various analytically derived relationships between ion-driven sputter/etch yield, U_{sb}, YM, and $\langle r\rangle$ carry some validity based on simple physical intuition. Specifically, a direct relation between sputter yield and the mechanical rigidity of the target material makes intuitive sense as YM represents the resistance to deformation by an applied force. The relation between sputter yield and hardness is perhaps even more intuitive given that hardness is defined as the resistance to plastic deformation when exposed to a compressive load (such as from a high-energy projectile). Similarly, the ultimate connection between U_{sb} and $\langle r\rangle$ makes intuitive sense since U_{sb} is a direct function of the number of bonds that must be broken in order for an atom to be removed from the surface. Therefore, as $\langle r\rangle$ decreases,

U_{sb} should decrease and sputter yield/etch rate should increase, as experimentally observed in this study.

Beyond reactive ion etching and sputtering, these results have additional important implications for the design and development of plasma-facing materials in nuclear fusion and fission reactors [68], as well as radiation hardened materials for microelectronic devices operating in defense, nuclear, and outer space applications [69-72]. For such materials, a resistance to ion-induced atomic displacements or a high tolerance for radiation-induced defects is desirable. The former is related to ion-induced etching or sputtering except that instead of all connecting bonds being broken at the surface, only a few bonds within the bulk of the material are disrupted [73,74]. This again implies a correlation between radiation hardness, bond energy, mechanical rigidity, and mean network coordination as observed here for ion sputtering and reactive ion etching. In fact, recent molecular dynamic simulations by Wang have shown that ion irradiation of SiO_2 can directly induce a topological transition from an over-constrained/stressed-rigid state to an under-constrained/flexible state [75].

Based on our observations, one would expect (in the absence of chemical reactivity) radiation hardness to increase with increasing degrees of over-constraint. In this regard, we note that recent investigations by Su et al have shown that the addition of carbon to SiO_2 glasses substantially improves the radiation hardness of this material [76,77]. Due to the higher coordination of carbon relative to oxygen, the addition of carbon to these glasses significantly increases the mean network coordination $\langle r \rangle$ and thus likely contributes to their improved radiation hardness. Thus, maximizing $\langle r \rangle$ can be generally viewed as important for optimizing the radiation hardness of amorphous materials.

VIII. CONCLUSIONS

In conclusion, we have demonstrated that a direct correspondence between surface binding energy (U_{sb}), Young's modulus (YM), and mean atomic coordination ($\langle r \rangle$) exists for mixed ionic–covalent materials that can be utilized to account for the properties of the target in various ion–solid interactions such as physical sputtering and reactive ion etching (RIE). These relations should prove particularly useful for understanding and predicting the ion–solid responses of multi-element, amorphous, and/or hydrogenated materials where YM and $\langle r \rangle$ are more experimentally accessible properties. The connection demonstrated between RIE rates and $\langle r \rangle$ further allows the underlying roll of atomic structure on ion–solid interactions to be better understood.

IX. ACKNOWLEDGEMENTS

This material is based upon work supported by the National Science Foundation under Grant No. DMR-1729227 and Intel Corporation under Contract No. 2012-IN-2313.

paquettem@umkc.edu, sean.king@intel.com

[1] G.S. Oehrlein, M.F. Doemling, B.E.E. Kastenmeier, P.J. Matsuo, N.R. Rueger, M. Schaepkens, and T.E.F.M. Standaert, IBM J. Res. Develop. 43, 181 (1999).
[2] L.M. Garrison, S.J. Zenobia, B.J. Egle, G.L. Kulcinski, and J.F. Santarius, Rev. Sci. Instrum. 87, 083502 (2015).
[3] W.E. Lee, M. Gilbert, S.T. Murphy, and R.W. Grimes, J. Amer. Ceram. Soc. 96, 2005 (2013)
[4] S.A. Thibeault, J.H. Kang, G. Sauti, C. Park, C.C. Fay, and G.C. King, MRS Bull. 40, 836 (2015).
[5] M.W. Thompson, Phys. Rep. 69, 335 (1981).
[6] H. Abe, M. Yoneda, and N. Fujiwara, Jpn. J. Appl. Phys. 47, 1435 (2008).
[7] Y. Kudriavstev, A. Villegas, A. Godines, and R. Asomoza, Appl. Surf. Sci. 239, 273 (2005).
[8] V.I. Zaporozchenko, M.G. Stepanova, and S.S. Vojtusik, Vacuum 47, 421 (1996).
[9] J.B. Malherbe, S. Hofmann, and J.M. Sanz, Appl. Surf. Sci. 27, 355 (1986).
[10] C. Boehme and G. Lucovsky, J. Appl. Phys. 88, 6055 (2000).
[11] N.W. Aschcroft and N.D. Mermin, *Solid State Physics* (Rinehart and Winston, New York 1976).
[12] J.C. Phillips and M. Thorpe, Sol. Stat. Comm. 53, 699 (1985).
[13] P. Boolchand and M. Thorpe, Phys. Rev. B 50, 10366 (1994).
[14] S. Dhungana, B.J. Nordell, A.N. Caruso, M.M. Paquette, W.A. Lanford, K. Scharfenberger, D. Jacob, and S.W. King, J. Vac. Sci. Technol. A 34, 061302 (2016).
[15] J. Mahan and A. Vantomme, Phys. Rev. B 61, 8516 (2000).
[16] P. Cortona, Phys. Rev. B 46, 2008 (1992).
[17] F. Aqra, Physica B 441, 54 (2014).
[18] T. Gorecki, Mat. Sci. Engr. 43, 225 (1980).
[19] C. Kittel, *Introduction to Solid State Physics, 8th Ed.* (Wiley, New York, 2005)
[20] J. Speight, *Langes Handbook of Chemistry, Vol. 16* (McGraw-Hill Ed., New York, 2005).
[21] D.A. Drabold, Eur. Phys. J. B 68, 1 (2009).
[22] J.Y. Kim, M.S. Hwang, Y.-H. Kim, H.J. Kim, Y. Lee, J. Appl. Phys. 90, 2469 (2001)
[23] P. Sigmund, Phys. Rev. 184, 383 (1969).
[24] M.P. Seah, C.A. Clifford, F.M. Green, and I.S. Gilmore, Surf. Interface. Anal. 37, 44, (2005).
[25] J.E. Mahan and A. Vantomme, J. Vac. Sci. Technol. A 15, 1976 (1997).

[26] H.M. Urbassek, Nucl. Instr. and Meth. B 18, 587 (1987).
[27] S.F. Belykh, V.I. Matveev, I.V. Veryovkin, A. Adriaens, and F. Adams, Nucl. Instr. and Meth. B 155, 409 (1999).
[28] N. Matsunami, Y. Yamamura, Y. Itikawa, N. Itoh, Y. Kazumata, S. Miyagawa, K. Morita, R. Shimizu, and H. Tawara, At. Data Nucl. Data Tables 31, 1 (1984).
[29] L.E. Rehn, R.C. Birtcher, S.E. Donnelly, P.M. Baldo, and L. Funk, Phys. Rev. Lett. 87, 207601 (2001).
[30] P.R. Barry, P. Philipp, T. Wirtz, and J. Kieffer, J. Mass. Spectrometry 49, 185 (2014).
[31] R.T. Poole, Am. J. Phys. 48, 536 (1980).
[32] S. Wacke, T. Gorecki, Cz. Gorecki, and K. Ksiazek, J. Phys.: Conf. Ser. 289, 012020 (2011).
[33] T.A. Pomorski, B.C. Bittel, P.M. Lenahan, E. Mays, C. Ege, J. Bielefeld, D. Michalak, and S.W. King, J. Appl. Phys. 115, 234508 (2014).
[34] M. Darnon, N. Casiez, T. Chevolleau, G. Dubois, W. Volksen, T. Frot, R. Hurand, T.L. David, N. Posseme, N. Rochat, C. Licitra, J. Vac. Sci. Technol. B 31, 11207 (2013).
[35] P. Lazzeri, X. Hua, G.S. Oehrlein, M. Barozzi, E. Iacob, M. Anderle, J. Vac. Sci. Technol. B 23, 1491 (2005).
[36] M.R. Baklanov, K.P. Mogilnikov, V.G. Polovinkin, F.N. Dultsev, J. Vac. Sci. Technol. B 18, 1385 (2000).
[37] S. King, R. Chu, G. Xu, J. Huening, Thin Solid Films 518, 4898 (2010).
[38] W.A. Lanford, M. Parenti, B.J. Nordell, M.M. Paquette, A.N. Caruso, M. Mantymaki, J. Hamalainen, M. Ritala, K.B. Klepper, V. Miikkulainen, O. Nilsen, W. Tenhaeff, N. Dudney, D. Koh, S.K. Banerjee, E. Mays, J. Bielefeld, and S.W. King, Nucl. Instr. Meth. B 371, 211 (2016).
[39] S. King, J. Bielefeld, G. Xu, W.A. Lanford, Y. Matsuda, R.H. Dauskardt, N. Kim, D. Hondongwa, L. Olasov, B. Daly, G. Stan, M. Liu, D. Dutta, and D. Gidley, J. Non-Cryst. Sol. 379, 67 (2013).
[40] D.L. Flamm and V.M. Donnelly, Plasma Chem. Plasma Proc. 1, 317 (1981).
[41] T.E.F.M. Standaert, C. Hedlund, E.A. Joseph, G.S. Oehrlein, T.J. Dalton, J. Vac. Sci. Technol. A 22, 53 (2004).
[42] N.R. Rueger, J.J. Beulens, M. Schaepkens, M.F. Doemling, J.M. Mirza, T.E.F.M. Standaert, G.S. Oehrlein, J. Vac. Sci. Technol. A 15, 1881 (1997).
[43] M. Schaepkens, T.E.F.M. Standaert, N.R. Rueger, P.G.M. Sebel, G.S. Oehrlein, J. Vac. Sci. Technol. A 17, 26 (1999).
[44] T.E.F.M. Standaert, M. Schaepkens, N.R. Rueger, P.G.M. Sebel, G.S. Oehrlein, J. Vac. Sci. Technol. A 16, 239 (1998).
[45] C. Li, R. Gupta, V. Pallem, G.S. Oehrlein, J. Vac. Sci. Technol. A 34, 031306 (2016).
[46] Y.A. Mankelevich, E.N. Voronina, T.V. Rakhimova, A.P. Palov, D.V. Lopaev, S.M. Zyryanov, M.R. Baklanov, J. Phys. D 49, 345203 (2016).
[47] A. Sankaran, M.J. Kushner, Appl. Phys. Lett. 82, 1824 (2003).
[48] I. Reid, G. Hughes, Semicond. Sci. Tech. 21, 1354 (2006).
[49] S.A. Vitale, H.H. Sawin, J. Vac. Sci. Technol. A 20, 651 (2002).
[50] R. Saha, W.D. Nix, Acta Mater. 50, 23 (2002).
[51] See Supplemental Material at [*URL will be inserted by publisher*) for a-SiN_x:H and a-SiO_xC_y:H etch rate correlations to mass density.
[52] H. Fan, C. Hartshorn, T. Buchheit, D. Tallant, R. Assink, R. Simpson, D.J. Kissel, D.J. Lacks, S. Torquato, C.J. Brinker, Nat. Mater. 6, 418 (2007).
[53] D. Music, U. Kreissig, Zs. Czigany, U. Helmersson, J.M. Schneider, Appl. Phys. A 76, 269 (2003).
[54] B.J. Nordell, S. Karki, T.D. Nguyen, P. Rulis, A.N. Caruso, S.S. Purohit, H. Li, S.W. King, D. Dutta, D. Gidley, W.A. Lanford, M.M. Paquette, J. Appl. Phys. 118, 035703 (2015).
[55] W. Gerhard, Z. Physik B 22, 31 (1975).
[56] N. Kuboi, T. Tatsumi, H. Minari, M. Fukasawa, Y. Zaizen, J. Komachi, and T. Kawamura, J. Vac. Sci. Technol. A 35, 061306 (2017).
[57] M. Plucinski, J.W. Zwanziger, J. Non-Cryst. Sol. 429, 20 (2015).
[58] M. Micoulaut, Adv. Phys. X 1, 147 (2016).
[59] P. Boolchand, X. Feng, W.J. Bresser, J. Non-Crystl. Sol. 293, 348 (2001).
[60] M.M. Paquette, B.J. Nordell, A.N. Caruso, M. Sato, H. Fujiwara, and S.W. King, MRS Bulletin 42, 39 (2017).
[61] H. He, M. Thorpe, Phys. Rev. Lett. 54, 2107 (1985).
[62] D. Franzblau, J. Tersoff, Phys. Rev. Lett. 68, 2172 (1992).
[63] J.N. Hernandez-Charpak, K.M. Hoogeboom-Pot, Q. Li, T.D. Frazer, J.L. Knobloch, M. Tripp, S.W. King, E.H. Anderson, W. Chao, M.M. Murnane, H.C. Kapteyn, and D. Nardi, Nano Lett. 17, 2178 (2017).
[64] R. Vogelgesang, M. Grimsditch, J.S. Wallace, Appl. Phys. Lett. 76, 982 (2000).
[65] W.C. Oliver, G.M. Pharr, J. Mater. Res. 7, 1564 (1992).
[66] H.J. McSkimin, J. Appl. Phys. 24, 988 (1953).
[67] H. Gokan, A. Morimoto, M. Murahata, Thin Solid Films 149, 85 (1987).
[68] J.B.O. Caughman, R.H. Goulding, T.M. Biewer, T.S. Bigelow, I.H. Campbell, J. Caneses, S.J. Diem, A. Fadnek, D.T. Fehling, R.C. Isler, E.H. Martin, C.M. Parish, J. Rapp, K. Wang, C.J. Beers, D. Donovan, N. Kafle, H.B. Ray, G.C. Shaw, M.A. Showers, J. Vac. Sci. Technol. A 35, 03E114 (2017)..
[69] D. Tang, I. Martin-Bragado, C. He, H. Zang, C. Xiong, Y. Li, D. Guo, P. Zhang, and J. Zhang, Micro. Rel. 60, 25 (2016).

[70] N. Kishimoto, H. Amekura, K. Kono, and C.G. Lee, J. Nuc. Mater. 258, 1908 (1998).
[71] M. Kisa, L. Li, J. Yang, T.K. Minton, W.G. Stratton, P. Voyles, X. Chen, K. van Benthem, and S.J. Pennycook, J. Spacecraft and Rockets 43, 431 (2006).
[72] T.K. Minton, B. Wu, J. Zhang, N.F. Lindholm, A.I. Abdulagatov, J. O'Patchen, S.M. George, and M.K. Groner, ACS Appl. Mater. Inter. 2, 2515 (2010).
[73] D. Simeone, J.M. Costantini, L. Luneville, L. Desgranges, P. Trocellier, and P. Garcia, J. Mater. Res. 30, 1495 (2015).
[74] E.M. Bringa, J.D. Monk, A. Caro, A. Misra, L. Zepeda-Ruiz, M. Duchaineau, F. Abraham, M. Nastasi, S.T. Picraux, Y.Q. Wang, and D. Farkas, Nano Lett. 12, 3351 (2012).
[75] B. Wang, N.M. Anoop Krishnan, Y. Yu, M. Wang, Y. Le Pape, G. Sant, and M. Bauchy, J. Non-Cryst. Sol. 463, 25 (2017).
[76] Q. Su, B. Cui, M. Kirk, and M. Nastasi, Phil. Mag. Lett. 96, 60 (2016).
[77] Q. Su, S. King, L. Li, T. Wang, J. Gigax, L. Shao, W.A. Lanford, M. Nastasi, Scr. Mater. 146, 316 (2018).